Published in final edited form as:

Nature. 2019 September ; 573(7772): 69–74. doi:10.1038/s41586-019-1485-8.

Mechanosensation of Cyclical Force by PIEZO1 is Essential for Innate Immunity

Angel G. Solis[1], **Piotr Bielecki**[1], **Holly R. Steach**[1], **Lokesh Sharma**[2], **Christian C. D. Harman**[3], **Sanguk Yun**[4], **Noah W. Palm**[1], **Marcel R. de Zoete**[5], **James N. Warnock**[6], **S. D. Filip To**[7], **Autumn G. York**[1], **Matthias Mack**[8], **Martin A. Schwartz**[4], **Charles. S. Dela Cruz**[2], **Ruaidhrí Jackson**[1,10], **Richard A. Flavell**[1,9,10]

[1]Department of Immunobiology, Yale University School of Medicine, New Haven, CT 06520, USA [2]Department of Internal Medicine, Pulmonary, Critical Care and Sleep Medicine, Yale School of Medicine, New Haven, CT 06520, USA [3]Department of Genetics, Yale University School of Medicine, New Haven, CT 06520, USA [4]Department of Internal Medicine, Yale Cardiovascular Research Center, Yale University, New Haven, CT 06520, USA [5]Department of Infectious Diseases and Immunology, Utrecht University, Utrecht, Netherlands [6]School of Chemical, Materials and Biomedical Engineering, University of Georgia, Athens GA, 30602, USA [7]Department of Agricultural and Biological Engineering, Mississippi State University, Mississippi State, MS 39759, USA [8]Department of Internal Medicine II – Nephrology, University Hospital Regensburg 93042 Regensburg, Germany [9]Howard Hughes Medical Institute, Yale University, New Haven, CT 06520, USA

Abstract

Although cells of the immune system experience force and pressure throughout their lifecycle, almost nothing is known about how these mechanical processes regulate the immune response[1]. Both tissue-resident and tissue-infiltrating immune cells in highly mechanical organs, such as the lung, are constantly exposed to tonic and dynamically changing mechanical cues[2]. Here using reverse genetics, we show that myeloid cells respond to force and alterations in cyclical hydrostatic pressure via the mechanosensory ion channel PIEZO1[3]. Unbiased RNA sequencing from macrophages subjected to cyclical hydrostatic pressure reveals a striking state of proinflammatory reprogramming. We report a novel mechanosensory-immune signaling circuit which PIEZO1 initiates in response to cyclical hydrostatic pressure, driving c-JUN activation and transcriptional upregulation of Endothelin-1 (EDN1). EDN1 in turn stabilizes HIF1α, which facilitates transcription of a potent and prolonged program of proinflammatory mediators. Using mice conditionally deficient of PIEZO1 in myeloid cells, and cellular depletion assays, we show

[10]Correspondence to: R.J. ruaidhri.jackson@yale.edu or R.A.F. richard.flavell@yale.edu.

Contributions

A.G.S. designed and performed experiments, collected and analyzed data, and wrote the manuscript. P.B. performed microbiological experiments and offered vital conceptual insight. H.R.S. developed reagents and performed Cas9 experiments. L.S. performed *in vivo* fibrosis experiments. C.C.D.H performed all bioinformatical analysis. S.Y. performed *in vitro* shear stress experiments. N.W.P. and M.R.D.Z generated mice and offered conceptual insight. J.N.W. and S.D.F.T. designed and built the bioreactor and software necessary to complete mechanistic experiments. A.G.Y. helped collect samples. M.M. provided critical reagents and advice on experimental design. M.A.S. and C.S.D.C. provided intellectual support. R.J. and R.A.F supervised the project, helped interpret the work, and supervised writing of the manuscript.

infiltrating monocytes respond to cyclical force to recruit neutrophils and clear pulmonary *Pseudomonas aeruginosa* infection via EDN1. Furthermore, myeloid PIEZO1 also drove lung pathology in a mouse model of pulmonary fibrosis. Our results demonstrate a novel environmental sensory axis that myeloid cells recognize to mount an inflammatory response and is the first report showing a physiological role for PIEZO1 and mechanosensation in immunity.

Mechanosensation in mammals affects and regulates a wide variety of processes including neuronal cell pain sensation[4], epithelial cell division[5,6], and endothelial cell-mediated vasodilation[7]. These mechanical cues signal through a class of proteins on the plasma membrane known as mechanosensory ion channels (MSICs)[3,8]. To investigate the capability of myeloid cell mechanosensation, we first asked if macrophages express any MSICs. Bone-marrow derived macrophages (BMDMs) show high expression of PIEZO1, an ion channel with high affinity for calcium[9–11], and negligible levels of other reported MSICs (Fig. 1a). To test the biological response to physical force in macrophages, cells were placed in a bioreactor capable of subjecting cells to cyclical hydrostatic pressure[12]. This pressure chamber consists of solenoid intake and exhaust valves to control timing of the pressure cycle, and is connected to a gas tank filled with 5% CO_2 balanced in air (Extended Data Fig. 1a). Therefore, the levels of O_2 and CO_2 experienced by cells in the chamber remain relatively constant throughout their stimulation, not accounting for physiological changes in pO_2 or pCO_2. The pressure chamber was housed inside a tissue culture incubator to equilibrate the chamber to 37°C. BMDMs grown in an adherent monolayer were then subjected to cyclical hydrostatic pressure at an amplitude of 15 mmHg, cycling once per second from 45 mmHg to 60 mmHg (Extended Data Fig. 1b). These parameters were chosen as they approximate the physiological parameters within the lung[13]. As a control, cells were placed in the chamber at a constant noncyclic pressure (at 45 mmHg), which we term static pressure (Extended Data Fig. 1b). Because PIEZO1-deficiency is embryonically lethal[14], we crossed Piezo1-floxed mice ($Piezo1^{fl/fl}$) to a LysM-driven Cre to delete PIEZO1 in myeloid cells. BMDMs from $Piezo1^{\Delta LysM}$ had an approximately 95% reduction in *Piezo1* mRNA compared to $Piezo1^{fl/fl}$ cells (Extended Data Fig. 1c). BMDMs from $Piezo1^{fl/fl}$ and $Piezo1^{\Delta LysM}$ mice were subjected to cyclical hydrostatic pressure for 6 hours. RNA was isolated and RNA-seq analysis was conducted. Cyclical hydrostatic pressure triggered robust upregulation of an array of proinflammatory genes, such as *Il1b, Cxcl10,* and *Ptgs2* in $Piezo1^{fl/fl}$-derived macrophages (Fig. 1b). Strikingly, however, this transcriptional reprogramming was completely abrogated in $Piezo1^{\Delta LysM}$ BMDMs (Fig. 1c), demonstrating that PIEZO1 signaling is essential for macrophage mechanosensation to cyclical hydrostatic pressure. We then independently validated the most upregulated genes by qPCR and ELISA (Fig. 1d–f). Furthermore, as increasing the overall magnitude of static pressure to 60 mmHg failed to induce transcriptional reprograming, we conclude that macrophage PIEZO1 is responding to cyclical hydrostatic pressure rather than overall magnitude of force (Extended Data Fig. 1d–e). Additionally, bone marrow monocytes were isolated and purified by negative magnetic bead selection. Importantly, monocytes displayed a similar transcriptional reprogramming as observed in BMDMs following cyclical hydrostatic pressure treatment, indicating a conserved PIEZO1-mediated mechanosensation signaling-axis in myeloid cells. (Fig. 1g). Given the fact that *Il1b* was transcriptionally upregulated following PIEZO1 signaling, we investigated if cyclical hydrostatic pressure influenced inflammasome

activation. Canonically, the NLRP3 inflammasome is first primed, usually via LPS, to transcriptionally upregulate *Il1b* and *Nlrp3*[15]. The primed inflammasome is then activated via a second signal that leads to Ca^{2+} influx and K^+ efflux[15]. It is therefore possible that PIEZO1-signaling can substitute for either or both signals. However, cyclical hydrostatic pressure alone was not able to induce IL-1β release in the absence of either LPS or nigericin (Extended Data Fig. 1f). This is likely caused by the inability of cyclical hydrostatic pressure to transcriptionally upregulate *Nlrp3* itself (Fig. 1b–c). Taken together, these results indicate that myeloid cells are capable of sensing cyclical hydrostatic pressure alterations in their environment via PIEZO1, and they functionally integrate this signal to drive a potent and selective proinflammatory response even in the absence of classical pathogen associated molecular patterns (PAMPs).

In order to investigate the mechanistic signaling program(s) that underlies this proinflammatory activation state, we first examined potential transcription factors that could explain such gene upregulation. Interestingly, we observed that a number of the upregulated genes were hypoxia inducible factor 1α (HIF1α) targets[16–20]. Indeed, BMDMs from $Piezo1^{fl/fl}$ mice displayed potent accumulation of HIF1α protein 4 to 6 hours after cyclical hydrostatic pressure stimulation (Fig. 1h). Importantly, HIF1α accumulation was completely absent in $Piezo1^{\Delta LysM}$ BMDMs following the cyclical hydrostatic pressure stimulation. Furthermore, upon mechanical stimulation, HIF1α translocated to the nucleus only in $Piezo1^{fl/fl}$ BMDMs (Fig. 1i). To test the role of HIF1α on the observed transcriptional reprogramming, we crossed $Hif1a^{fl/fl}$ to LysM-Cre mice. HIF1α-deficient macrophages showed complete abrogation of the cyclical hydrostatic pressure induced transcriptional reprograming at 6 hours (Fig. 1j). In normoxic conditions, HIF1α hydroxylation by prolyl hydroxylases (PHDs) marks HIF1α for ubiquitination via Von Hippel Lindau tumor suppressor (VHL) E3 ubiquitin ligase, and ultimately, degradation[21]. To investigate if the pressure chamber generated a hypoxic environment, we used pimonidazole, which forms a detectable product only in the absence of oxygen[22]. BMDMs cultured for 6 hours in hypoxic conditions (2% O_2) showed a clear increase in detectable pimonidazole, yet no HIF1α stabilization was observed at this relatively early timepoint[23] (Extended Data Fig. 2a). In contrast, no detectable pimonidazole was detected following static or cyclical hydrostatic pressure conditions (Extended Data Fig. 2b). We also tested if hypoxic conditions could recapitulate our observed transcriptional upregulation of proinflammatory genes, or synergize with PIEZO1 signaling. Neither hypoxic conditions alone nor cyclical hydrostatic pressure in hypoxic conditions affected the transcriptional response of these PIEZO1-inducible genes (Extended Data Fig. 2c). Therefore, we conclude that the observed HIF1α accumulation must be caused by either protein stabilization or transcriptional upregulation in a hypoxia-independent manner. As no differences in *Hif1a* mRNA levels following cyclical hydrostatic pressure were observed (Extended Data Fig. 2d), we conclude that PIEZO1-signaling results in HIF1α protein stabilization.

We next sought to determine how PIEZO1-signaling results in HIF1α stabilization. We first investigated if cyclical hydrostatic pressure inhibits PHD enzymes globally. However, in contrast to HIF1α stabilization, cyclical hydrostatic pressure does not trigger HIF2α accumulation (Extended Data Fig. 2e). Therefore, we conclude that recognition of cyclical hydrostatic force by myeloid cells specifically regulates HIF1α-degradation. As acidity is

known to induce HIF1α stabilization[24], we tested if PIEZO1-signaling altered pH. Using the cell-permeable pH sensor pHrodo Red AM and a pH meter in the supernatant of cells exposed to cyclical hydrostatic pressure stimulation, we observed no difference in intracellular or extracellular acidity, respectively (Extended Data Fig. 3a–b). PIEZO1 is known to function as an ion channel facilitating calcium-influx into the cytoplasm[9–11]. In order to test if PIEZO1-dependent calcium influx was the driver of HIF1α in BMDMs, cells were subjected to cyclical hydrostatic pressure either in calcium-free media or with the addition of the PIEZO1 inhibitor GsmT×4[25]. The HIF1α signal was completely abrogated in both conditions suggesting PIEZO1 mediates HIF1α accumulation via Ca^{2+} influx in response to cyclical hydrostatic pressure (Fig. 2a). Furthermore, we were able to remove the reversible PIEZO1 inhibitor GsmT×4 from the cells by washing with media and observed restoration of HIF1α stabilization, indicating an operative role for the PIEZO1 channel in Ca^{2+} influx dependent stabilization (Extended Data Fig. 4a). Indeed, as depletion of intracellular calcium stores with the cell-permeable calcium chelator BAPTA-AM had no effect on cyclical hydrostatic pressure induced HIF1α stabilization (Extended Data Fig. 4b), we conclude that Ca^{2+} derived from the extracellular space via plasma membrane PIEZO1 is required for HIF1α stabilization.

To test if an intrinsic PIEZO1-mediated Ca^{2+} signaling pathway or a secreted soluble factor was required for HIF1α stabilization, we performed supernatant transfer experiments. In brief, $Piezo1^{fl/fl}$ and $Piezo1^{\Delta LysM}$ BMDMs were cultured for 6 hours under cyclical hydrostatic pressure, then supernatant was collected, clarified, and placed on fresh cells in static pressure for 2 hours. Supernatant from cyclical hydrostatic pressure treated $Piezo1^{fl/fl}$ BMDMs was capable of inducing HIF1α in both $Piezo1^{fl/fl}$ and $Piezo1^{\Delta LysM}$ macrophages (Fig. 2b). Conversely, supernatant from cyclical hydrostatic pressure treated $Piezo1^{\Delta LysM}$ derived macrophages did not have the ability to induce HIF1α stabilization in either $Piezo1^{fl/fl}$ or $Piezo1^{\Delta LysM}$ BMDMs. Additionally, the factor capable of inducing HIF1α stabilization was still present when supernatants were passed through a column that excludes molecules larger than 10 kDa (Fig. 2b). Furthermore, treatment with brefeldin A (BFA), which prevents vesicle trafficking from the ER to the Golgi[26], prevented secretion of the factor responsible for HIF1α stabilization (Fig. 2b). Indeed, we were able to wash BFA from media and observe restoration of HIF1α 2 hours following removal (Extended Data Fig. 4c). Taken together, this data excludes a mechanism whereby PIEZO1-Ca^{2+} signaling directly stabilizes HIF1α during cyclical hydrostatic pressure sensation. Instead, it favors a model in which PIEZO1-Ca^{2+} signaling drives expression of a small secretory molecule with the capacity to stabilize HIF1α.

We therefore re-examined the RNA-seq data and searched for suitable gene targets that were upregulated by cyclical hydrostatic pressure, smaller than 10 kDa, and released by the secretory system. Endothelin-1 (EDN1) is a hormone discovered to cause vasoconstriction in endothelial cells[27]. PIEZO1-signaling resulted in a robust upregulation and secretion of EDN1 (Fig. 2c–d). Translation of *Edn1* mRNA results in a 212-amino acid peptide which ultimately is processed by furin-like proteases[28] and endothelin converting enzymes[29] into a biologically-active 21-amino acid peptide[30]. Active EDN1, therefore, is smaller than 10 kDa, and its secretion is blocked by BFA[31]. EDN1 has also been observed to induce HIF1α stabilization in pulmonary artery smooth muscle cells *in vitro*[32]. *Edn1* mRNA upregulation

occurred as quickly as 1 hour following cyclical hydrostatic pressure stimulation (Fig. 2c) and recombinant EDN1 stabilized HIF1α in both Piezo1$^{fl/fl}$ and Piezo1$^{\Delta LysM}$ macrophages (Fig. 2e). Bosentan, an endothelin receptor antagonist[33], completely blocked HIF1α stabilization with cyclical hydrostatic pressure and prevented the observed transcriptional reprogramming at 6 hours of mechanostimulation (Fig. 2f–g). Mechanistically, EDN1 has been shown to stabilize HIF1α by activating calcineurin, a phosphatase which dephosphorylates RACK1[32]. RACK1 phosphorylation is necessary to bring HIF1α in contact with E3 ubiquitin ligase complex responsible for its subsequent proteasomal degradation[34]. To test if this mechanism is relevant in cyclical hydrostatic pressure stimulated macrophages, we used cyclosporine A (CsA), an inhibitor of calcineurin[32]. Treatment with CsA during cyclical hydrostatic pressure treatment resulted in a loss of HIF1α stabilization, suggesting that the reported mechanism is conserved in macrophages during the sensation of cyclical hydrostatic pressure (Fig. 2h). In agreement with this data, inhibition of proteasomal degradation using MG132, a proteasomal inhibitor[35], but not chloroquine, a lysosomal acidification inhibitor[36], rescued HIF1α stabilization in Piezo1$^{\Delta LysM}$ BMDMs (Extended Data Fig. 4d).

We next sought to understand the initial PIEZO1-dependent signaling pathway which drives the primary EDN1 upregulation (Fig. 2c). We tested if HIF1α was necessary and saw that Hif1a$^{\Delta LysM}$ macrophages had no loss of EDN1 at this early timepoint (Extended Data Fig. 4e). Cyclical mechanotransduction has previously been reported to activate EDN1 expression via AP-1 through an unknown sensory mechanism[37]. At early timepoints of cyclical hydrostatic pressure, we observed PIEZO1-dependent increases in JNK and c-JUN phosphorylation (Fig. 2i). Pharmacological inhibition of AP-1 resulted in loss of HIF1α stabilization at 6 hours post-mechanostimulation (Fig. 2j). Furthermore, inhibition of AP-1 also resulted in loss of *Edn1* mRNA levels at 1h and 6h of cyclical hydrostatic pressure treatment (Fig. 2k). Interestingly, however, treatment with echinomycin, an inhibitor of HIF1α-DNA interactions, only resulted in loss of *Edn1* at 6h timepoint (Fig. 2k), indicating that AP-1 is the early driver of EDN1, and HIF1α is a late driver required to potentiate the proinflammatory transcriptional program. In fact, HIF1α stabilization alone via PHD inhibitor DMOG is insufficient to drive the transcriptional response in the absence cyclical hydrostatic pressure (Extended Data Fig. 4f–g). Indeed, pretreatment of BMDMs with cyclical hydrostatic pressure for 2 hours prior to DMOG treatment resulted in a synergistic upregulation of HIF1α target genes over mechanostimulation alone. This indicates that cyclical hydrostatic pressure stimulation is a prerequisite for the HIF1α-dependent program (Extended Data Fig. 4f–g). Finally, using BMDMs from Cas9-knockin mice (Cas9-KI)[38], we disrupted key genes in the proposed signaling pathway to genetically validate the mechanism independently from pharmacological strategies. Single guide RNAs were cloned into a retroviral vector, and subsequent transduction of Cas9-KI macrophages resulted in targeted indel formation and gene inactivation[39]. Guide RNAs targeting Piezo1, cJun, Edn1, Endothelin receptor B (Ednrb), or Hif1a resulted in a complete abrogation of cyclical hydrostatic pressure induced transcriptional reprogramming (Fig. 2l). Importantly however, guide RNAs targeting the B-cell specific gene CD79a and Endothelin receptor A (Ednra) which are not expressed in macrophages, have no effect on cyclical hydrostatic pressure-mediated transcriptional reprogramming indicating Cas9-mediated activity itself does not

impact the pathway (Fig. 2l). These results identify a PIEZO1-dependent mechanism of early AP-1 activation in response to cyclical hydrostatic pressure that drives Endothelin-1 transcription. EDN1 signaling triggered HIF1α stabilization, which in turn facilitates prolonged proinflammatory mediator expression. Taken together, we have elucidated a novel biological circuit that links mechanosensation to innate immunity.

Next, we sought to uncover if PIEZO1 was required for host defense during a physiological bacterial infection. As the lung is an organ where cells experience high amounts of mechanical stimulation[2], and as *Pseudomonas aeruginosa* infection results in alterations of the mechanical properties of the lung[40], we chose this model to investigate the physiological role of PIEZO1 in innate immunity. Indeed, alveolar macrophages and monocytes isolated from the lung of steady state and *P. aeruginosa* infected mice highly express *Piezo1* (Extended Data Fig. 5a–b). Therefore, we infected Piezo1$^{fl/fl}$ and Piezo1$^{\Delta LysM}$ mice with 5×10^6 colony forming units (CFUs) of *P. aeruginosa* via intranasal instillation. Following 24 hours of intranasal infection with *P. aeruginosa*, Piezo1$^{\Delta LysM}$ showed higher bacterial loads in lung and liver than wild-type littermates, demonstrating an inability to control bacterial infection, and prevent systemic dissemination (Fig. 3a–b). We next asked if there may be differences in cellular recruitment to the lung at early timepoints of infection. Because the lung is a highly vascularized organ, we used *in vivo* labeling with α-CD45.2 to separate immune cells in circulation from infiltrated/tissue-protected immune cells[41]. Interestingly, we observed decreased numbers of tissue-infiltrating neutrophils in Piezo1$^{\Delta LysM}$ mice 6 hours post-infection compared to Piezo1$^{fl/fl}$ mice, but no difference in monocyte levels. (Fig. 3c–d, Extended Data Fig. 6a–c). At 2 hours post-infection, Piezo1$^{\Delta LysM}$ bronchoalveolar lavage fluid (BALF) contained significantly decreased levels of inflammatory mediators, previously shown to be PIEZO1-inducible in monocytes and BMDMs *in vitro*, compared to Piezo1$^{fl/fl}$ mice (Fig. 3e).

In order to investigate if this heightened proinflammatory response was due to stabilized HIF1α, we examined both tissue-resident macrophages, which have been exposed to tonic cyclical hydrostatic pressure throughout their life cycle, and newly recruited myeloid cells, which have no previous exposure to mechanical force. We infected Piezo1$^{fl/fl}$ and Piezo1$^{\Delta LysM}$ mice with *P. aeruginosa* for 6 hours and analyzed intracellular HIF1α levels from cells in the lung. Interestingly, only infiltrated monocytes showed robust upregulation of HIF1α in Piezo1$^{fl/fl}$ mice. (Fig. 3f, Extended Data Fig. 6d). Importantly, HIF1α upregulation in Piezo1$^{\Delta LysM}$ monocytes was significantly reduced (Fig. 3f). Furthermore, circulating monocytes showed no Hif1α accumulation in either Piezo1$^{fl/fl}$ or Piezo1$^{\Delta LysM}$ after infection (Extended Data. Fig. 6e). As previous reports have shown that extravasation alone can result in immune cell activation *in vitro*[42], the observed HIF1α stabilization could conceivably be triggered by force exerted on monocytes during the process of extravasation, or by the hydrostatic pressure microenvironment encountered by monocytes upon recruitment to the lung. To test this, we infected mice with *P. aeruginosa* intraperitoneally, and saw no upregulation of HIF1α in peritoneal recruited monocytes (Extended Data. Fig. 6f). This observation demonstrates that the shear stress provoked by extravasation is not sufficient to induce HIF1α stabilization in monocytes. Furthermore, macrophages subjected to oscillatory shear stress *in vitro* upregulated *Icam1* (Extended Data Fig. 6g), an important molecule for cellular adhesion that has previously been shown to be regulated by shear

force[42]. However, *Icam1* transcriptional upregulation was independent of PIEZO1 (Extended Data Fig. 6g). Importantly, as oscillatory shear stress did not upregulate the PIEZO1-dependent program of proinflammatory genes (Extended Data Fig. 6g), we conclude that distinct mechanical forces regulate divergent transcriptional responses through independent mechanosensors and molecular signaling pathways.

We next tested if PIEZO1-dependent Endothelin-1 production played a critical role in antibacterial defense *in vivo*. EDN1 levels have already been shown to be increased in pulmonary disease[43,44], and affect parasitic infection[45]. Interestingly, although *P. aeruginosa* infection triggered EDN1 in BALF 2 hours post-infection in Piezo1$^{fl/fl}$ mice, Piezo1$^{\Delta LysM}$ animals had no detectable EDN1 (Fig. 3g). To test if alveolar macrophages were a major source of EDN1, we crossed Piezo1$^{fl/fl}$ with mice expressing Cre-recombinase under the control of CD11c, which results in efficient deletion in alveolar macrophages and dendritic cells[46]. Piezo1$^{\Delta CD11c}$ showed no reduction in EDN1 levels in BALF 2 hours post-infection with *P. aeruginosa*, implying that PIEZO1 plays no role in EDN1 expression from alveolar macrophages or dendritic cells (Fig. 3g). Therefore, as neutrophils do not express PIEZO1 (Extended Data Fig. 5c), we hypothesized that monocytes likely played a critical role in the PIEZO1-mediated production of EDN1 expression. To test this possibility, we administered a monoclonal antibody against CCR2, previously described to deplete monocytes efficiently[47]. Monocyte depletion resulted in significant loss of EDN1 from the BALF compared to isotype control 6 hours after bacterial infection (Fig. 3h). Furthermore, we also identify monocytes as a major cellular source of neutrophil chemoattractant CXCL2 (Fig. 3h), which is also a PIEZO1-dependent gene following mechanostimulation (Fig. 1b). Next we asked if EDN1 was required for *P. aeruginosa* clearance. Mice administered with an α-EDN1 antibody showed increased levels of lung and liver bacterial abundance 24 hours after *P. aeruginosa* infection compared to isotype control (Fig. 3i, Extended Data Fig. 7a). In order to test if EDN1 could rescue Piezo1$^{\Delta LysM}$ mice from susceptibility to infection, recombinant EDN1 was administered intranasally, and we observed decreased levels of lung and liver bacteria 24 hours post-infection compared to vehicle treated mice (Fig. 3j, Extended Data Fig. 7b). Furthermore, pharmacological antagonism of endothelin receptors also resulted in susceptibility to bacterial infection (Extended Data Fig. 7c–d). Taken together, we show that PIEZO1 is essential for myeloid cell-mediated protection from *P. aeruginosa* and is vital for EDN1 production and HIF1α activation in newly recruited monocytes which in turn drive neutrophil recruitment and pathogen clearance.

Given its importance in pathogen-induced inflammation, we sought to investigate if PIEZO1 mediated myeloid cell activation could also drive autoinflammatory disease associated with mechanical perturbations in the lung. Bleomycin-induced pulmonary fibrosis results in aberrant alterations of the lung mechanical environment[48] and it has been shown that myeloid cells impact pathology significantly[49]. We observed protection from bleomycin-induced lung damage in Piezo1$^{\Delta LysM}$ mice as measured by Ashcroft scoring of pathohistology[50], and reduced levels of Endothelin-1 from BALF (Fig. 3k–m). Therefore, PIEZO1 is not only relevant in pulmonary infection, but also plays a physiologically important role in driving pathology during autoinflammatory processes such as pulmonary fibrosis.

We have unequivocally shown for the first time a mechanism that allows myeloid cells to sense their physical environment and integrate this signal to drive innate immune activation. Specifically, PIEZO1 signaling primes myeloid cells toward a proinflammatory profile dependent on AP-1 activation, EDN1 expression, and HIF1α stabilization (Extended Data Fig. 8). Furthermore, we have shown PIEZO1-mediated mechanosensation is essential for physiological protection against bacterial infection within the lung and can drive robust pathological tissue damage during pulmonary fibrosis. We identify that infiltrating lung monocytes respond to cyclical hydrostatic pressure with HIF1α stabilization and secretion of molecules, such as EDN1, and neutrophil chemoattractant CXCL2 (Extended Data Fig. 9). This demonstrates the possibility that PIEZO1 may be a novel therapeutic target for treatment of pulmonary fibrotic autoinflammatory diseases. Taken together, this work is the first to show force as a novel parameter than can alter immune cell function, and is likely relevant in other cells, organs, diseases, and immunological processes.

Methods

Animals

Piezo1$^{fl/fl}$ embryonic stem (ES) cells were obtained from the KnockOut Mouse Project (KOMP) Repository. ES cells were injected into a blastocyst, and the F1 generation were backcrossed to C57Bl/6 mice to obtain homozygous-floxed mice. Mice were then crossed to LysM-Cre mice obtained from Jackson Laboratories. Experimental groups of mice were obtained by crossing homozygous Piezo1$^{fl/fl}$; homozygous Cre-negative to homozygous Piezo1$^{fl/fl}$; heterozygous Cre-positive mice, which would produce an equal number of Cre-negative and Cre-positive mice. All experiments were performed using littermate control, cohoused mice. All animal experimentation was performed in compliance with Yale Institutional Animal Care and Use Committee protocols.

Generation of BMDMs

Mice were sacrificed and hind legs were removed and placed in conical tubes containing 5% FCS DMEM media (Gibco). Muscle was removed from tibia and femur bones and the ends of bones were cut off. Using a 271/2 gauge needle, 10 mL of sterile DMEM media supplemented with 10% FBS, pen/strep, and L-glutamine was passed through the bone. Cells were pelleted and plated with mouse MCSF (50 ng/mL) (BioLegend). Following 4 days of incubation, supernatant was removed and plated in a new dish. Cells were again incubated in media with mouse MCSF for 3 more days. Dishes were then washed 3 times with sterile PBS to remove unadhered cells. BMDMs were gently scraped off the dish, pelleted, counted, and seeded in new plates for experimentation. In the case of experiments with calcium-free medium, immediately prior to experimentation, cells were washed three times with PBS, before adding calcium-free DMEM (Gibco) with pen/strep and L-glutamine. Controls for calcium-free medium experiment were placed in calcium-sufficient DMEM with pen/strep and L-glutamine. In some experiments, cells were treated with DMOG (200 μM), GsmT×4 (5 μM), Brefeldin-A (3 μg/mL), recombinant EDN1 (conc), Bosentan (10 μM), Cyclosporine A (10 μM), SR 11302 (10 μM), Echinomycin (5 nm), Bapta-AM (10 μM), Chloroquine (100 μM) or MG132 (50 μM)

RNA Isolation and Processing

BMDMs were plated at 1–2×10^6 cells per well on a flat bottom non-adherent 12-well plates. Following treatment, cells were washed once with PBS, and gently dislodged from the plate with PBS. Cells were pelleted and then processed using Qiagen RNeasy Mini Plus Kit (Qiagen) using the manufacturer's protocol. RNA quantity was assayed using a NanoDrop Microvolume Spectrophotometer (Thermo). RNA was sent for RNA-sequencing or converted to cDNA using Maxima H Minus Reverse Transcriptase Kit and using the manufacturer's protocol (Thermo). qPCR was conducted using Sigma KiCqStart predesigned SYBR green primers and iTaq™ Universal SYBR® Green Supermix (Bio-Rad). Relative mRNA amounts were compared to *Gapdh* mRNA levels. mRNA for RNAseq analysis was purified using PolyA$^+$ selection and processed by the Yale Center for Genome Analysis using standard methodology and sequenced on a HiSeq2000 with 75bp pair-ended reads.

RNAseq Analysis

Fragments were mapped to the mouse genome (mm9) with Tophat2 using default parameters. A reference transcriptome consisting of UCSC known genes was used for isoform-level quantification and differential analysis using Cuffdiff2. Quality control analysis and visualization were done using the CummeRbund package, which is part of the R/Bioconductor suite of utilities. Differentially expressed genes between samples were selected with a Benjamini-Hochberg corrected p-value < 0.05 deemed by the Cuffdiff2 program as significant. Volcano plots were generated using Origin Software and Heatmaps were generating using Morpheus by Broad Institute.

Pressure Chamber

All pressure chamber experiments used a custom-built pressure chamber bioreactor built from the lab of Dr. James Warnock. The chamber computational board was connected to a laptop running custom software designed and coded on LabVIEW. The air intake valve was connected to a regulated gas tank containing 5% CO_2 balanced in air (21% O_2, 79% N_2), except in the case of hypoxia synergy studies, where a gas tank containing 2% O_2, rather than 21% O_2, was substituted. The chamber was placed inside a tissue culture chamber to allow temperatures to reach 37°C. The program parameters were set such that the air intake valve would be open for 0.6s, then the exhaust valve would be opened for 0.4s at a sampling rate of 10 samples per second. The regulator on the gas tank was adjusted such that the amplitude of cyclical hydrostatic pressure was approximately 15mmHg, and adjustments were made constantly throughout the experiments to maintain this amplitude. For static pressure control experiments, both the air intake and exhaust valve were opened, and the regulator was adjusted such that the pressure within the chamber reached the lower parameter achieved in the corresponding cyclical hydrostatic pressure experiment, unless otherwise noted.

ELISA

BMDM supernatants were centrifuged at 13,000g for 10 minutes to remove cellular debris. ELISA measurements were conducted using kits for CXCL10, EDN1, IL-1β (R&D DuoSets), or PGE2 (R&D Parameter Assay).

Western Blotting

BMDMs were washed on ice with ice cold PBS, then lysed over 30 minutes with ice cold RIPA Lysis Buffer containing a cocktail of protease inhibitors (Roche) and phosphatase inhibitors (NEB) with gentle agitation every 10 minutes. Cellular debris was clarified (13,000g, 10 minutes, 4°C). Reducing agent (NuPAGE Thermo) and Sample Buffer was added to supernatant, and boiled at 95°C for 10 minutes. Protein lysates were resolved on NuPAGE™ 4–12% Bis-Tris Protein Gels using MOPS running buffer (Invitrogen), transferred to nitrocellulose membrane, and blocked with 5% OmniBlok™ Dry Milk in PBS. Detection of HIF1α (D2U3T), Hif2α (D9E3), phospho-c-JUN (54B3 and 9164), phospho-JNK (81E11), total c-JUN (60A8) and total JNK (9252) was conducted using monoclonal antibodies (Cell Signaling). β-tubulin (E7) was detected using a monoclonal antibody (DSHB). HRP-conjugated anti-rabbit (Cell Signaling, 7074) or anti-mouse antibody (GE Healthcare, NA931V) was used as secondary antibodies and detected using SuperSignal West Pico PLUS Chemiluminiscent Substrate (Thermo) and autoradiography film (Denville).

Confocal Microscopy

For HIF1α detection, BMDMs were fixed with 4% methanol free paraformaldehyde for 10 minutes and permeablized with 0.3% Triton X for 30 minutes. Cells were blocked with 2% BSA 0.1% Triton X and stained with a monoclonal Rabbit anti-HIF1α antibody (Cell Signaling, D1S7W). Cells were then washed, stained with a polyclonal anti-rabbit secondary (Life Technologies), and imaged with a Nikon-Ti microscope combined with UltraVox spinning disk (PerkinElmer) and data was analyzed using the Volocity software (PerkinElmer).

Intracellular pH Assay

Intracellular pH was measured using cell-permeable pHrodo red AM intracellular pH sensor (Invitrogen). Macrophages were subjected to cyclical hydrostatic pressure. In the final 30 minutes of mechanostimulation, cells were washed according to the manufacturer's protocol and pHrodo dye was added. As a control, cells were incubated in the absence of mechanostimulation in acidic DMEM (pH 6.5). Cells were then washed again on ice and immediately analyzed via flow cytometry.

Oscillatory Shear Stress

Macrophages were plated on plastic slides coated with fibronectin (20 μg/ml) for two days. The slides were mounted into parallel plate flow chambers and subjected to oscillatory flow (1 ± 5 dynes/cm^2, 1 Hz) for 6 hours. Flow was applied using a syringe pump (NE1050, New Era Pump Systems) combined with a peristaltic pump (Masterflex C/L, Cole Palmer) for

media circulation. Media was maintained at 37°C using a temperature control system (Cole Palmer) and infused with 5% CO_2.

sgRNA cloning and Retroviral Production

MGguide was modified to contain an Escherichia coli phenylalanyl-tRNA synthetase a-subunit (ePheS) negative selection cassette and to express human NGFR (Addgene) under control of the SV40 promoter. To clone individual sgRNA, the vector was digested with BbsI, eliminating the ePheS cassette, and annealed oligonucleotides with complementary overhangs were ligated into the vector using T4 DNA ligase (NEB). STBL3 cells (Invitrogen) were transformed and grown on plates and in media containing 16 mM 4-Chloro-DL-phenylalanine (Alfa Aesar) and Ampicillin. For retroviral production, 7E6 293T cells were plated in a 10 cm dish and the following day were transfected with 5.3 ug of MG-guide and 2.6 ug of EcoHelper plasmid (Addgene) using LipoD293 transfection reagent. At 24 hours media was replaced, and at 48 hours supernatants were collected.

CRISPR Knockout

CRISPR/Cas9 knockout experiments were carried out using a modified version of a previously published protocol. Briefly, bone marrow from Cas9-transgenic mice was harvested and cultured in complete DMEM with MCSF (50 ng/mL) in non-tissue culture treated dishes. 24 hours later, media was replaced with MG-guide retroviral supernatants supplemented with MCSF. Three days later, BMDMs were detached using Accutase (Sigma # A6964–100ML) and live CD11b-positive cells were FACS sort-purified based on hNGFR reporter expression using the following reagents: biotin labelled anti-human CD271 (BD biosciences), BV421 labelled Streptavidin (Biolegend), BV711 labelled anti-CD11b (Biolegend), Fixable Viability Dye eFluor 780 (ThermoFisher). Sorted cells were plated in 24 well plates at 5×10^5 cells per mL in media containing MCSF.

Pseudomonas aeruginosa Infection

P. aeruginosa (PA14 strain kindly provided by Dr. Barbara Kaczmierczek, Yale University) was maintained as a glycerol stock at −80°C. One day prior to infection, bacteria was grown at 37°C in a shaking incubator for approximately 16 hours in LB media. Bacteria were subcultured in a 1:20 ratio in a volume of 20mL until OD600 was between 1.5 and 2.0, which is approximately 1.5×10^9 and 2×10^9 CFUs/mL. A dose of 2.5×10^8 CFUs was diluted in 1mL of sterile PBS, washed twice (8000 rpm, 2 minutes), and diluted to a final volume of 1mL. Mice were anesthetized with methoxyflurane, and a dose of 5×10^6 CFUs was instilled intranasally using a micropipette. Following infection, mice were sacrificed and lungs and liver were dissected using sterile techniques and placed in a sterile gentleMACS tissue dissociator tube (Miltenyi Biotec). Prior to tissue dissociation via a gentleMACS tissue dissociator, 2 mL of sterile PBS was added. Homogenate was diluted in serial 10-fold dilutions in sterile PBS and plated on LB plates in triplicate. Total CFUs were counted and CFUs/g was calculated.

In Vivo Labeling of CD45.2$^+$ Cells

Mice were anesthetized using isoflurane and intravenously injected with 100uL of PBS containing CD45.2-Pacific Blue antibody (Biolegend, clone 104, 1:40 dilution). After 5 minutes, mice were then sacrificed and samples were collected for flow cytometry as described below.

Lung Processing and Flow Cytometry

Mice were sacrificed, and lungs were removed and placed in fresh media on ice. Tissues were then finely chopped with clean dissection scissors, and digested with media containing collagenase D (1 mg/mL) (Sigma) and DNase I (Sigma) for 30 minutes to an hour. Cells were then filtered through a 70um filter and pelleted. Epithelial cells were removed using an 80% to 40% Percoll gradient (GE Healthcare) spun at 600g for 20 minutes with slow acceleration and no brake at room temperature. Cells between the gradient were removed and pelleted. Red blood cells were lysed using ACK Lysis Buffer (Vita Scientific). Cells were then stained for 30 minutes at 4°C in the dark using the following Biolegend antibodies: CD45.2 (clone 104), TCRβ (clone H97–597), TCR γ/δ (clone GL3), NK1.1 (clone PK136), B220 (clone RA3–6B2), CD19 (clone 6D5), Ly6c (clone HK1.4), Ly6g (clone 1A8), CD169 (clone 3D6.112), Ter119 (clone Ly-76), CD90.2 (clone 53–2.1), CD11c (clone N418), SiglecF (R&D BAF1706), CD11b (clone M1/70). For intracellular staining, cells were fixed and permeablized using the Foxp3/Transcription Factor Staining Buffer Set (eBioscience™) exactly as described in the manufacturer's protocol. Intracellular HIF1α was probed using a monoclonal PE-conjugated antibody (CST, D1S7W). Cells were then filtered through a 40μM filter, and 20,000 counting beads (Invitrogen) were added. Samples were resuspended in PBS containing 2% FCS and 2mM EDTA and acquired with an LSRII cytometer (BD Bioscience) and analyzed using FlowJo (BD Bioscience).

Bronchoalveolar Lavage Fluid Molecular Measurement

Mice were sacrificed and the trachea was exposed surgically. A small incision was made into the trachea to allow a blunt-ended needle to be inserted and tied with sutures. Lungs were aspirated with 1 ml sterile PBS and placed in a 2 mL microcentrifuge tube on ice. Cells and cellular debris was removed by centrifugation (12,000g, 10 minutes, 4°C) and supernatants were analyzed for IL-6, IL-10, TNF, IL-33, IL-4, CXCL2 (R&D Duoset), and PGE2 (R&D Parameter Assay).

Hypoxia Studies

Differentiated BMDMs were plated in glass bottom 24-well plates and incubated for 6 hours either in static pressure, cyclic pressure, or in a hypoxia chamber (2% O_2, 5% CO_2, N_2). After 6 hours, cells were analyzed for transcriptional profile as described above. Pimonidazole (20μM, Hypoxyprobe) was added in the last hour of incubation, and cells were then fixed and permeablized using the Foxp3/Transcription Factor Staining Buffer Kit (eBioscience). Pimonidazole was detected using a monoclonal antibody conjugated to Cy7-conjugated (1:200, Hypoxyprobe). Confocal microscopy was conducted as described above.

Pulmonary Fibrosis

Lung fibrosis model was established using bleomycin (Zydus Hospira Oncology). Briefly, mice were anesthetized using 3% isoflurane and instilled with 1.5 U/Kg of bleomycin in 50 μl of PBS by intratracheal route using oropharyngeal aspiration. Mice were euthanized at 14 days post bleomycin, when there were obvious fibrotic changes in the lung. Histology sections were blindly scored following the Ashcroft Scoring system[50].

Extended Data

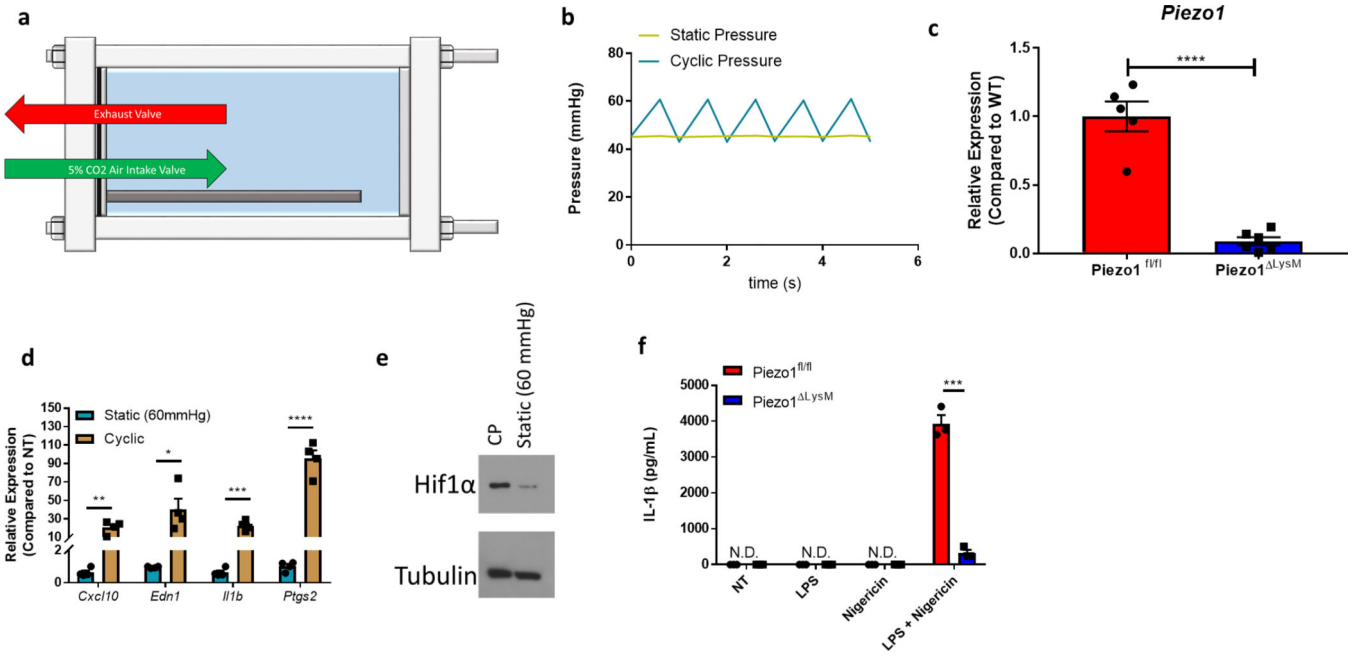

Extended Data Figure 1: Pressure Chamber Schematic and PIEZO1 Knockout Validation

a, Schematic of cyclical hydrostatic pressure bioreactor showing side view. **b,** Graph of pressure regimes used within the pressure chamber. **c**, qPCR analysis of *Piezo1* transcript in unstimulated BMDMs from Piezo1$^{fl/fl}$ (WT) and Piezo1$^{\Delta LysM}$ mice. Data is presented as 5 biological replicates from two independent experiments. **d**, qPCR analysis of Piezo1$^{fl/fl}$ BMDMs treated with static pressure at the indicated magnitude, or with cyclical hydrostatic pressure for 6 hours. Data is presented as 4 biological replicates from two independent experiments. **e**, Representative immunoblot analysis of HIF1α and β-tubulin from Piezo1$^{fl/fl}$ BMDMs treated with static pressure at the indicated magnitude, or with cyclical hydrostatic pressure for 6 hours. Data is representative of 2 independent experiments. **f,** ELISA analysis of IL-1β from Piezo1$^{fl/fl}$ and Piezo1$^{\Delta LysM}$ BMDMs treated with cyclical hydrostatic pressure alone (NT), LPS (10 ng/mL) for 5h in cyclical hydrostatic pressure followed by 1h cyclical hydrostatic pressure, 5h cyclical hydrostatic pressure followed by 1h nigericin (10 μM) in cyclical hydrostatic pressure, or LPS (10 ng/mL) for 5h followed by 1h nigericin (10 μM) with cyclical hydrostatic pressure. Data is presented as 3 biological replicates. **c,d,f** SEM of replicates is present and significance is determined by unpaired two-tailed T test (*p<0.05, **p<0.01, ***p<0.001, ****p<0.0001).

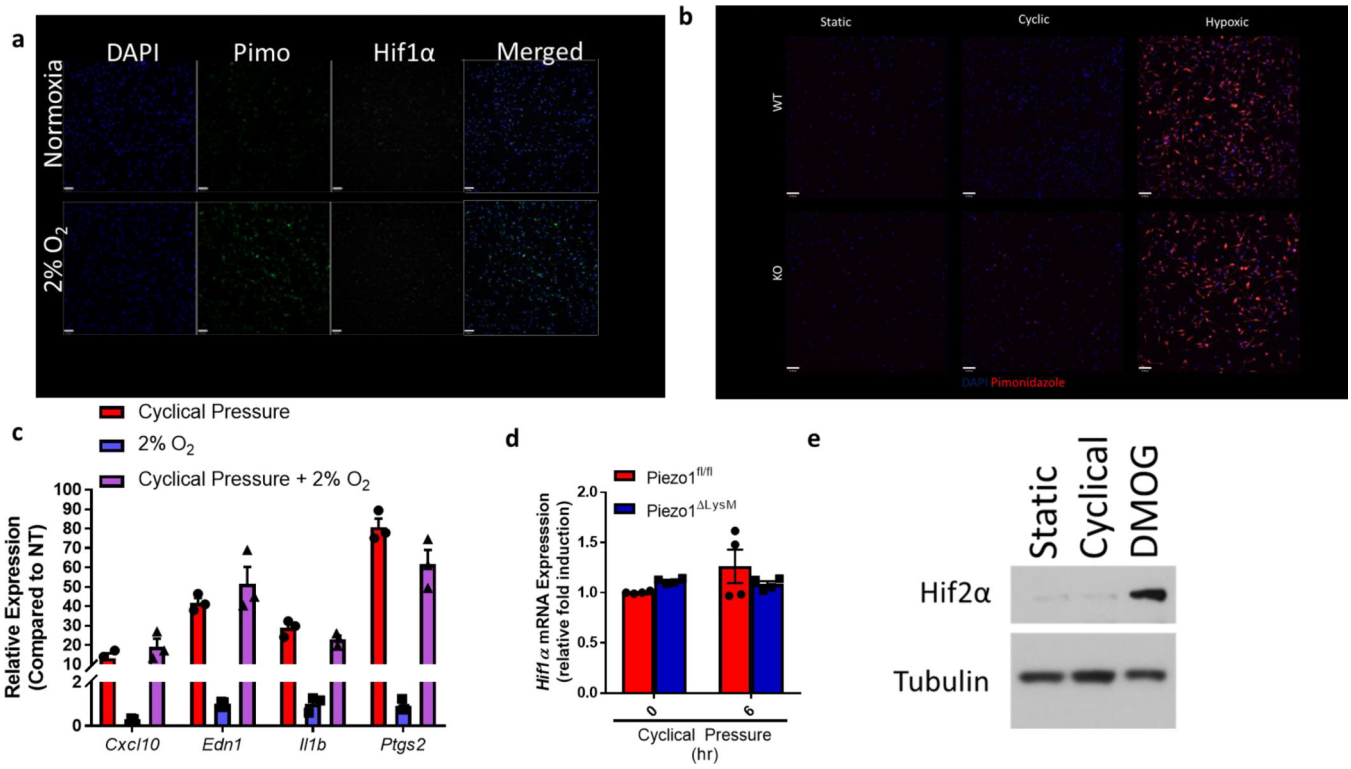

Extended Data Figure 2: HIF1α Stabilization is Hypoxia Independent During Cyclical Hydrostatic Pressure Stimulation

a, Representative confocal microscopy of BMDMs treated for 6 hours in either normoxic conditions or in a hypoxic chamber (2% O_2). Cells were treated with pimonidazole (20 μM) 1 hour prior to completion of treatment. Upon completion, cells were fixed, permeabilized, and stained with monoclonal antibody against pimonidazole. Data is representative of 2 independent experiments. **b**, Confocal microscopy of BMDMs treated for 6 hours in either static pressure, cyclical pressure, or hypoxic chamber (0.5% O_2). Cells were treated with pimonidazole (20 μM) 1 hour prior to completion of treatment. Upon completion, cells were fixed, permeabilized, and stained with monoclonal antibody against pimonidazole. Data is representative of 2 independent experiments. **c**, qPCR analysis of BMDMs treated with cyclical hydrostatic pressure, 2% O_2, or cyclical hydrostatic pressure with 2% O_2 for 6 hours. Data is presented as 3 biological replicates. **d**, qPCR analysis of *Hif1a*-mRNA in BMDMs following cyclical hydrostatic pressure. Data is presented as 4 biological replicates. Data is from 2 independent experiments. **e**, Representative immunoblot analysis of HIF2α and β-tubulin from BMDMs treated with static pressure, cyclical hydrostatic pressure, or DMOG (200 μM) for 6 hours. **b,c**, SEM of replicates is shown, and significance is determined by unpaired two-tailed t-test.

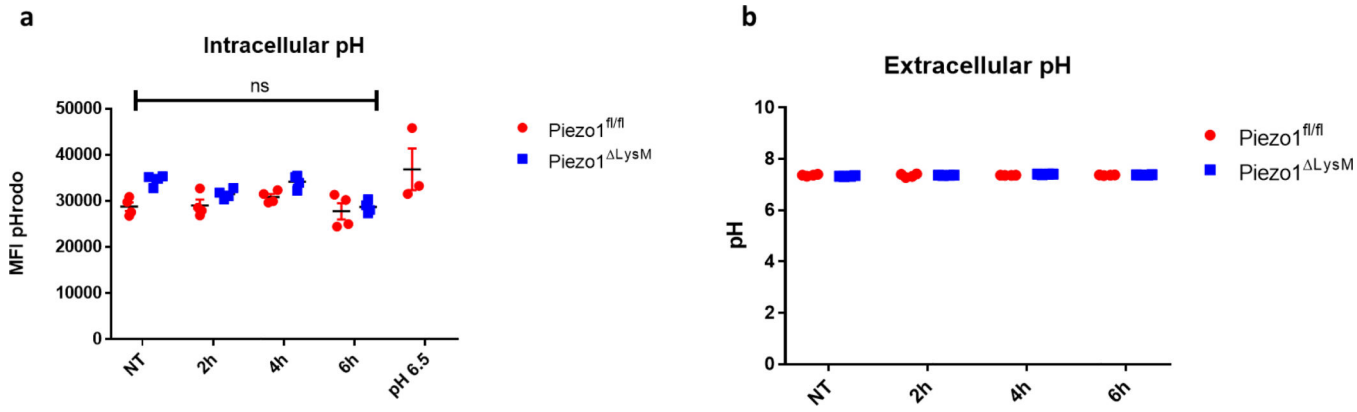

Extended Data Figure 3: Cyclical Hydrostatic Pressure Induced HIF1α Protein is Stabilized Independent of Acidity

a, Intracellular pH measurements using pHrodo intracellular pH indicator dye for final 30 minutes of treatment. Cells were treated with cyclical hydrostatic pressure for the indicated periods or with low pH cell medium for 6 hours. **a,b**, SEM of replicates is shown, and significance is determined by unpaired two-tailed t-test. **b**, pH measurements of supernatant taken with a pH electrode from BMDM culture treated with cyclical hydrostatic pressure for the indicated periods.

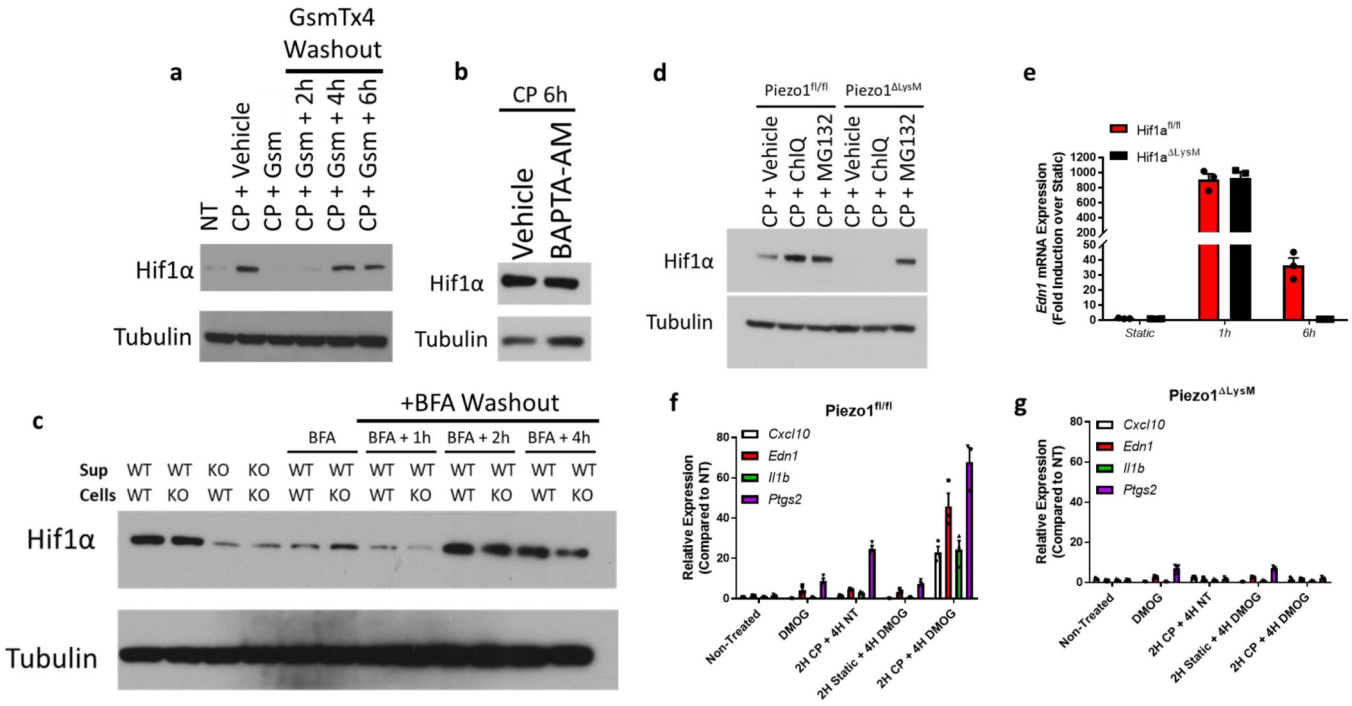

Extended Data Figure 4: Kinetics and Sufficiency of Cyclical Hydrostatic Pressure Induced HIF1α Stabilization and Transcriptional Response

a, Representative immunoblot analysis of HIF1α and β-tubulin from BMDMs in cyclical hydrostatic pressure with GsmT×4 (Gsm) (5 μM) for 6 hours, then washed three times in DMEM prior to further cyclical hydrostatic pressure stimulation. **b**, Representative immunoblot analysis of HIF1α and β-tubulin from BMDMs in cyclical hydrostatic pressure for 6 hours pretreated with BAPTA-AM (10 μM) for 30 minutes. Data is representative of 2 independent experiments. **c**, Representative immunoblot analysis of HIF1α and β-tubulin in BMDMs. Piezo1$^{fl/fl}$ (WT) or Piezo1$^{\Delta LysM}$ (KO) were cultured in cyclical hydrostatic pressure for 6 hours along with BFA (3 μg/mL). Cells were then washed with DMEM three times and further subjected to additional cyclical hydrostatic pressure stimulation. Supernatant (sup) was then clarified and transferred to WT or KO BMDMs cultured in static pressure for 2 additional hours. **d**, Representative immunoblot analysis of HIF1α and β-tubulin from cyclical hydrostatic pressure stimulated BMDMs treated with chloroquine (ChlQ, 100 μM) or MG132 (50 μM) for 6 hours with cyclical hydrostatic pressure. **e**, qPCR analysis of *Edn1* from Hif1a$^{fl/fl}$ and Piezo1$^{\Delta LysM}$ BMDMs treated with cyclical hydrostatic pressure for 1 and 6 hours. Data is presented as 3 biological replicates. **f-g**, qPCR analysis of (**f**) Piezo1$^{fl/fl}$ or (**g**) Piezo1$^{\Delta LysM}$ BMDMs cultured in 6 hours of DMOG treatment (200 μM), 6 hours of cyclical hydrostatic pressure (CP), 2 hours of cyclical hydrostatic pressure followed by 4 hours of no treatment (NT), 2 hours of static pressure followed by 4 hours DMOG (200 μM), or 2 hours cyclical hydrostatic pressure followed by 4 hours DMOG (200 μM). Data is representative of 3 biological replicates. SEM of replicates is shown.

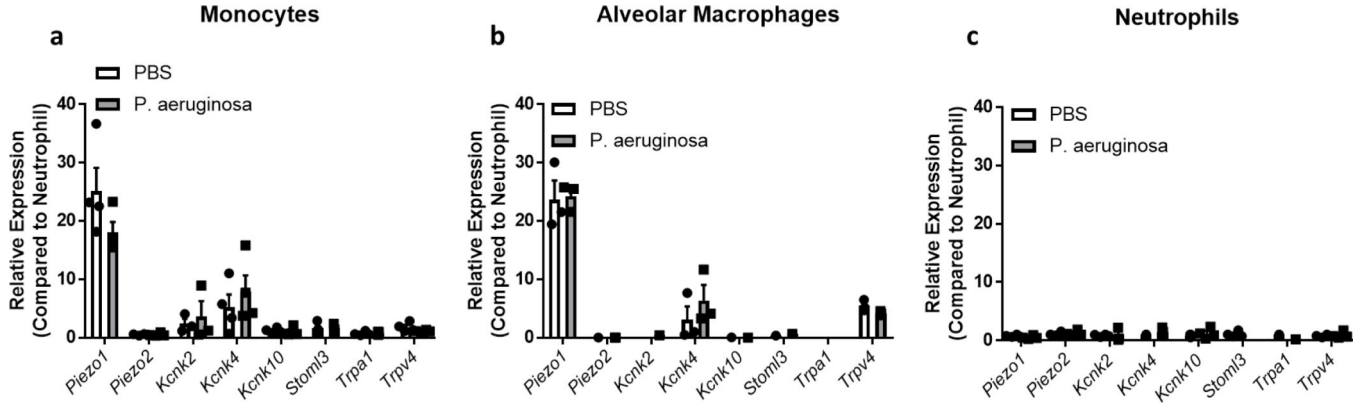

Extended Data Figure 5: Bacterial Infection Has No Effect on MSIC Expression

a-c, qPCR analysis of known mammalian mechanosensory ion channels from (**a**) monocytes, (**b**) alveolar macrophages, or (**c**) neutrophils sorted sorted from lung of mice infected with *P. aeruginosa* or PBS for 6 hours. Data is represented as fold increase over neutrophil expression for each gene. Data is representative of 4 biological replicates. SEM of replicates is shown.

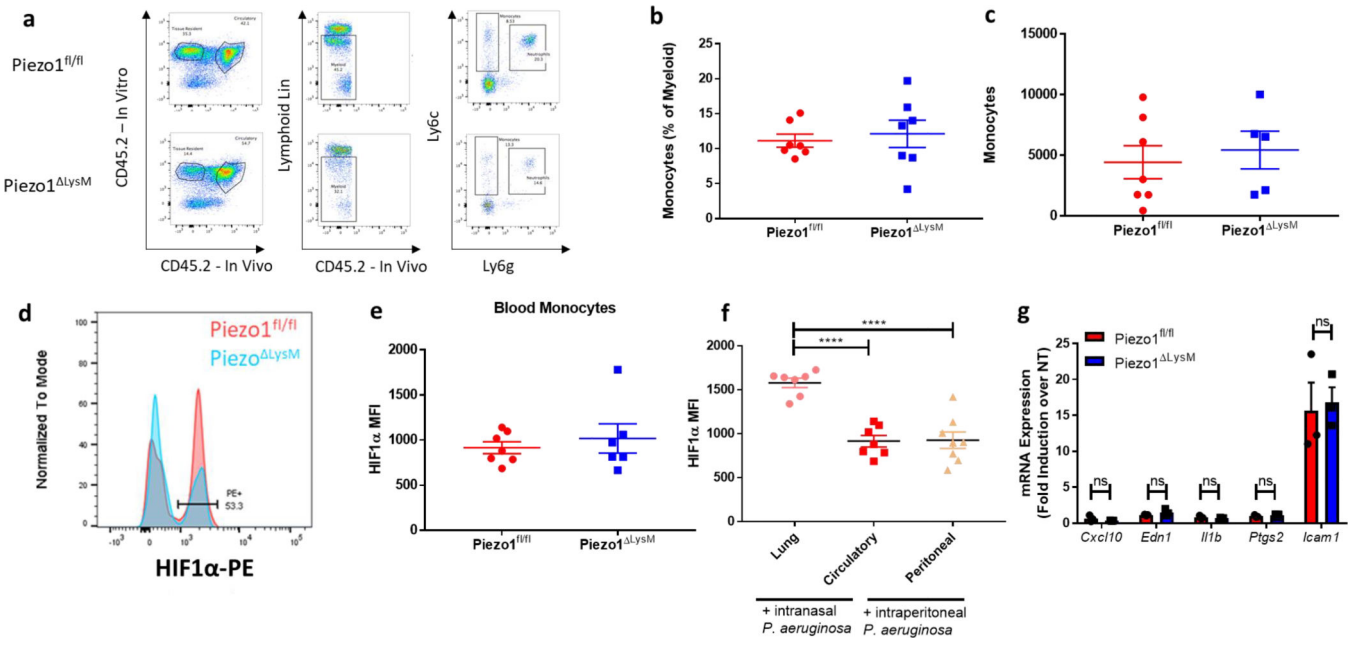

Extended Data Figure 6: PIEZO1-Dependent Cyclical Hydrostatic Pressure Stabilizes HIF1α in the Lung

a, Representative flow cytometry of lungs from Piezo1$^{fl/fl}$ (top) (n=9) or Piezo1$^{\Delta LysM}$ (bottom) (n=9) mice infected intranasally with *P. aeruginosa* for 6 hours. Lymphoid lineage consists of TCRβ, NK1.1, B220, CD19, CD90.2, and TCRγδ. Data is representative of 2 independent experiments. **b-c**, Infiltrating monocyte quantification in terms of (**b**) percentage and (**c**) total numbers following 6 hours of intranasal *P. aeruginosa* infection. Data is representative of 2 independent experiments. **d,** Representative intracellular flow cytometry histograms of HIF1α from total lung interstitial monocytes of Piezo1$^{fl/fl}$ and Piezo1$^{\Delta LysM}$ mice infected intranasally with *P. aeruginosa* for 6 hours. Data is from 2 independent experiments. **e**, Mean fluorescent intensity of HIF1α from *in vivo* labeled CD45.2+ circulatory monocytes from mice infected with *P aeruginosa* for 6 hours. Data is from 2 independent experiments. **f**, Mean fluorescent intensity of HIF1α from tissue-infiltrated and circulatory monocytes from mice infected with *P aeruginosa* intranasally or intraperitoneally for 6 hours. Data is from 2 independent experiments. **g**, qPCR analysis from BMDMs treated with oscillatory shear stress for 6 hours. Data is representative of 3 biological replicates. **c-g**, SEM of replicates is present and significance is determined by unpaired two-tailed T test (****p<0.0001).

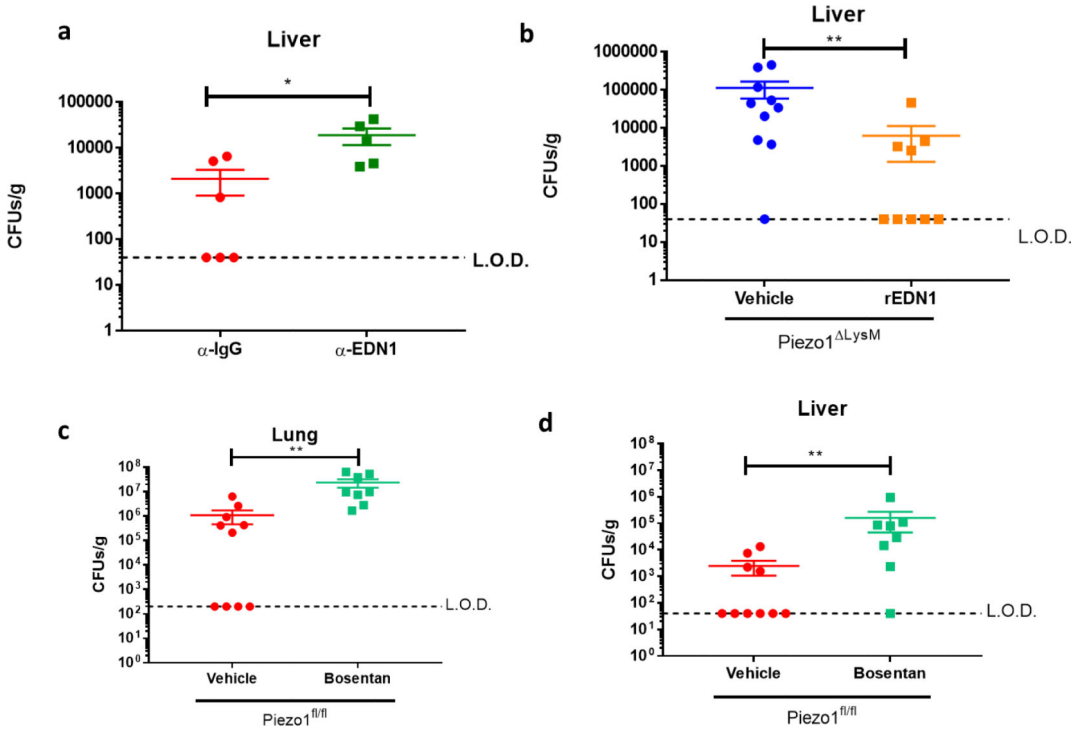

Extended Data Figure 7: Endothelin-1 Signaling Confers Protection to *P aeruginosa* Infection

a, CFUs from liver of Piezo1$^{fl/fl}$ mice infected intranasally with *P. aeruginosa* for 24 hours treated with α-EDN1 (ENDO20–2101.70, ThermoFisher) (25 μg) or isotype control intranasally 6 hours prior to infection. Data is from 2 independent experiments. **b,** CFUs from liver of Piezo1$^{\Delta LysM}$ mice infected intranasally with *P. aeruginosa* for 24 hours treated with vehicle (PBS) or Endothelin-1 (rEDN1)(10ug) at the time of infection. Data is from 2 independent experiments. **c-d,** CFUs from (**c**) lung or (**d**) liver of Piezo1$^{fl/fl}$ mice infected intranasally with P. aeruginosa for 24 hours treated with vehicle (DMSO) or bosentan (100 mg/kg) intraperitoneally 3 hours prior to infection. Data is from 2 independent experiments. SEM of replicates is shown, and significance is determined by unpaired Mann-Whitney U Test (*p<0.05,**p<0.01).

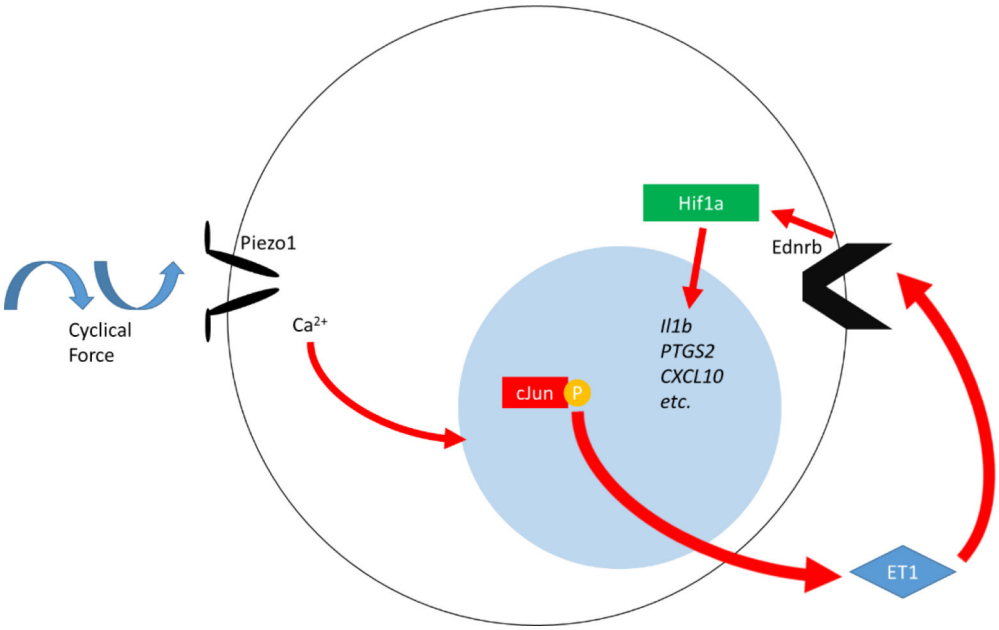

Extended Data Figure 8: PIEZO1 Recognition of Cyclical Force Drives a HIF1α Proinflammatory Program

Cyclical force signals via PIEZO1 in myeloid cells, resulting in Ca^{2+} influx and AP-1 induced EDN1 expression. Ednrb signaling then drives HIF1α stabilization and proinflammatory transcriptional upregulation.

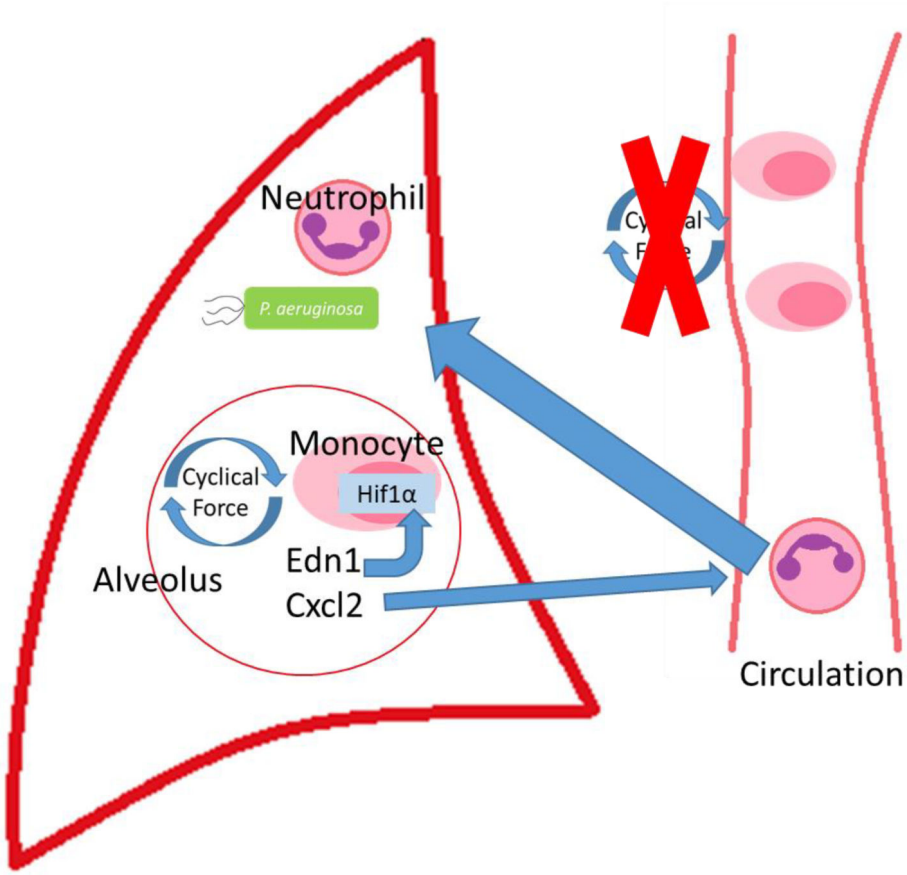

Extended Data Figure 9: Infiltrating Monocytes Recognize Cyclical Hydrostatic Pressure in the Lung Via PIEZO1 to Trigger Neutrophil Mediated Bacterial Clearance

Recruited monocytes recognize cyclical force via PIEZO1 in the lung and secrete EDN1 to drive HIF1α stabilization and CXCL2 expression to induce neutrophilia and bacterial clearance.

Acknowledgment

We would like to thank Jon Alderman, Caroline Lieber, Cynthia Hughes, Elizabeth Hughes-Picard, and Patricia Rainey for help in facilitating this work. We would like to thank Dr. Barbara Kazmierczak for providing the *P. aeruginosa* used in this work. We would like to thank Dr. Manolis Roulis for insightful comments and reagents used in this work. We would like to thank Lilla Orr for extremely helpful insight regarding statistical analysis. We would like to thank Dr. Ian Odell for his help regarding computational software. We would like to thank Dr. Carla Rothlin and Dr. Clara Abraham for continued support and feedback as this work progressed. We would like to thank Dr. Ping-Min Chen for help and reagents related to hypoxia studies. This work was supported in part by the Searle Scholars Program, the Leukemia Research Foundation, the Gruber Foundation, the NIH (R01GM122984). A.G.S. was in part supported by an NIH training grant (T32 GM007499) and the American Society for Microbiology. This work was supported in part by the Crohn's and Colitis Foundation of America (R.J.). This work was supported by the Howard Hughes Medical Institute and the Blavatnik Family Foundation (R.A.F.).

References

1. Huse M Mechanical forces in the immune system. Nat. Rev. Immunol 17, 679–690 (2017). [PubMed: 28757604]
2. McWhorter FY, Davis CT & Liu WF Physical and mechanical regulation of macrophage phenotype and function. Cell. Mol. Life Sci 72, 1303–1316 (2015). [PubMed: 25504084]

3. Coste B et al. Piezo1 and Piezo2 are essential components of distinct mechanically activated cation channels. Science 330, 55–60 (2010). [PubMed: 20813920]
4. Murthy SE et al. The mechanosensitive ion channel Piezo2 mediates sensitivity to mechanical pain in mice. Sci. Transl. Med 10, eaat9897 (2018). [PubMed: 30305457]
5. Gudipaty SA et al. Mechanical stretch triggers rapid epithelial cell division through Piezo1. Nature 543, 118–121 (2017). [PubMed: 28199303]
6. Eisenhoffer GT et al. Crowding induces live cell extrusion to maintain homeostatic cell numbers in epithelia. Nature 484, 546–549 (2012). [PubMed: 22504183]
7. Wang S et al. Endothelial cation channel PIEZO1 controls blood pressure by mediating flow-induced ATP release. J. Clin. Invest 126, 4527–4536 (2016). [PubMed: 27797339]
8. Delmas P, Hao J & Rodat-Despoix L Molecular mechanisms of mechanotransduction in mammalian sensory neurons. Nat. Rev. Neurosci 12, 139–153 (2011). [PubMed: 21304548]
9. Glogowska E et al. Novel mechanisms of PIEZO1 dysfunction in hereditary xerocytosis. Blood 130, 1845–1856 (2017). [PubMed: 28716860]
10. Retailleau K et al. Piezo1 in Smooth Muscle Cells Is Involved in Hypertension-Dependent Arterial Remodeling. Cell Rep. 13, 1161–1171 (2015). [PubMed: 26526998]
11. Miyamoto T et al. Functional Role for Piezo1 in Stretch-evoked Ca^{2+} Influx and ATP Release in Urothelial Cell Cultures. J. Biol. Chem 289, 16565–16575 (2014). [PubMed: 24759099]
12. Schipke KJ, To SDF & Warnock JN Design of a cyclic pressure bioreactor for the ex vivo study of aortic heart valves. J. Vis. Exp (2011). doi:10.3791/3316
13. Mead J & Whittenberger JL Physical Properties of Human Lungs Measured During Spontaneous Respiration. J. Appl. Physiol 5, 779–796 (1953).
14. Li J et al. Piezo1 integration of vascular architecture with physiological force. Nature 515, 279–282 (2014). [PubMed: 25119035]
15. He Y, Hara H & Núñez G Mechanism and Regulation of NLRP3 Inflammasome Activation. Trends Biochem. Sci 41, 1012–1021 (2016). [PubMed: 27669650]
16. Tannahill GM et al. Succinate is an inflammatory signal that induces IL-1β through HIF-1α. Nature 496, 238–42 (2013). [PubMed: 23535595]
17. Yamashita K, Discher DJ, Hu J, Bishopric NH & Webster KA Molecular Regulation of the Endothelin-1 Gene by Hypoxia. J. Biol. Chem 276, 12645–12653 (2001). [PubMed: 11278891]
18. Jung F, Palmer LA, Zhou N & Johns RA Hypoxic regulation of inducible nitric oxide synthase via hypoxia inducible factor-1 in cardiac myocytes. Circ. Res 86, 319–25 (2000). [PubMed: 10679484]
19. Lee JJ et al. Hypoxia activates the cyclooxygenase-2-prostaglandin E synthase axis. Carcinogenesis 31, 427–34 (2010). [PubMed: 20042640]
20. JUNG Y-J, ISAACS JS, LEE S, TREPEL J & NECKERS L IL-1β-mediated up-regulation of HIF-1α via an NFκB/COX-2 pathway identifies HIF-1 as a critical link between inflammation and oncogenesis. FASEB J. 17, 2115–2117 (2003). [PubMed: 12958148]
21. Palazon A, Goldrath AW, Nizet V & Johnson RS HIF transcription factors, inflammation, and immunity. Immunity 41, 518–28 (2014). [PubMed: 25367569]
22. Varia MA et al. Pimonidazole: A Novel Hypoxia Marker for Complementary Study of Tumor Hypoxia and Cell Proliferation in Cervical Carcinoma. Gynecol. Oncol 71, 270–277 (1998). [PubMed: 9826471]
23. Philip K et al. HIF1A up-regulates the ADORA2B receptor on alternatively activated macrophages and contributes to pulmonary fibrosis. FASEB J. 31, 4745–4758 (2017). [PubMed: 28701304]
24. Mekhail K, Gunaratnam L, Bonicalzi M-E & Lee S HIF activation by pH-dependent nucleolar sequestration of VHL. Nat. Cell Biol 6, 642–647 (2004). [PubMed: 15181450]
25. Bae C, Sachs F & Gottlieb PA The Mechanosensitive Ion Channel Piezo1 Is Inhibited by the Peptide GsMT×4. Biochemistry 50, 6295–6300 (2011). [PubMed: 21696149]
26. Fujiwara T, Oda K, Yokota S, Takatsuki A & Ikehara Y Brefeldin A causes disassembly of the Golgi complex and accumulation of secretory proteins in the endoplasmic reticulum. J. Biol. Chem 263, 18545–52 (1988). [PubMed: 3192548]

27. Yanagisawa M et al. A novel potent vasoconstrictor peptide produced by vascular endothelial cells. Nature 332, 411–415 (1988). [PubMed: 2451132]
28. Blais V et al. Processing of proendothelin-1 by members of the subtilisin-like pro-protein convertase family. FEBS Lett. 524, 43–8 (2002). [PubMed: 12135739]
29. Shimada K et al. Cloning and Functional Expression of Human Endothelin-Converting Enzyme cDNA. Biochem. Biophys. Res. Commun 207, 807–812 (1995). [PubMed: 7864876]
30. Stow LR, Jacobs ME, Wingo CS & Cain BD Endothelin-1 gene regulation. FASEB J. 25, 16–28 (2011). [PubMed: 20837776]
31. Shinagawa S et al. T cells upon activation promote endothelin 1 production in monocytes via IFN-γ and TNF-α. Sci. Rep 7, 14500 (2017). [PubMed: 29101349]
32. Li M et al. Endothelin-1 induces hypoxia inducible factor 1α expression in pulmonary artery smooth muscle cells. FEBS Lett. 586, 3888–3893 (2012). [PubMed: 23041290]
33. Roux S & Rubin LJ Bosentan: a dual endothelin receptor antagonist. Expert Opin. Investig. Drugs 11, 991–1002 (2002).
34. Liu YV et al. Calcineurin Promotes Hypoxia-inducible Factor 1α Expression by Dephosphorylating RACK1 and Blocking RACK1 Dimerization. J. Biol. Chem 282, 37064–37073 (2007). [PubMed: 17965024]
35. Baig MS et al. NOS1-derived nitric oxide promotes NF-κB transcriptional activity through inhibition of suppressor of cytokine signaling-1. J. Exp. Med 212, 1725–1738 (2015). [PubMed: 26324446]
36. Wolfram J et al. A chloroquine-induced macrophage-preconditioning strategy for improved nanodelivery. Sci. Rep 7, 13738 (2017). [PubMed: 29062065]
37. Cheng T-H et al. Reactive Oxygen Species Mediate Cyclic Strain-induced Endothelin-1 Gene Expression via Ras/Raf/extracellular Signal-regulated Kinase Pathway in Endothelial Cells. J. Mol. Cell. Cardiol 33, 1805–1814 (2001). [PubMed: 11603923]
38. Platt RJ et al. CRISPR-Cas9 Knockin Mice for Genome Editing and Cancer Modeling. Cell 159, 440–455 (2014). [PubMed: 25263330]
39. Shalem O et al. Genome-scale CRISPR-Cas9 knockout screening in human cells. Science 343, 84–87 (2014). [PubMed: 24336571]
40. Lindsey AS et al. Analysis of pulmonary vascular injury and repair during Pseudomonas aeruginosa infection-induced pneumonia and acute respiratory distress syndrome. Pulm. Circ 9, 2045894019826941 (2019). [PubMed: 30632898]
41. Novak J, Georgakoudi I, Wei X, Prossin A & Lin CP In vivo flow cytometer for real-time detection and quantification of circulating cells. Opt. Lett 29, 77–9 (2004). [PubMed: 14719666]
42. HSIAI TK et al. Monocyte recruitment to endothelial cells in response to oscillatory shear stress. FASEB J 17, 1648–1657 (2003). [PubMed: 12958171]
43. Chalmers GW et al. Sputum endothelin-1 is increased in cystic fibrosis and chronic obstructive pulmonary disease. Eur. Respir. J 13, 1288–92 (1999). [PubMed: 10445603]
44. Zheng L et al. Endothelin-1 in stable bronchiectasis. Eur. Respir. J 16, 146–9 (2000). [PubMed: 10933101]
45. Tanowitz HB et al. Role of Endothelin 1 in the Pathogenesis of Chronic Chagasic Heart Disease. Infect. Immun 73, 2496–2503 (2005). [PubMed: 15784596]
46. Abram CL, Roberge GL, Hu Y & Lowell CA Comparative analysis of the efficiency and specificity of myeloid-Cre deleting strains using ROSA-EYFP reporter mice. J. Immunol. Methods 408, 89–100 (2014). [PubMed: 24857755]
47. Mack M et al. Expression and characterization of the chemokine receptors CCR2 and CCR5 in mice. J. Immunol 166, 4697–704 (2001). [PubMed: 11254730]
48. Phillips JE et al. Bleomycin induced lung fibrosis increases work of breathing in the mouse. Pulm. Pharmacol. Ther 25, 281–285 (2012). [PubMed: 22024054]
49. Misharin AV et al. Monocyte-derived alveolar macrophages drive lung fibrosis and persist in the lung over the life span. J. Exp. Med 214, 2387–2404 (2017). [PubMed: 28694385]
50. Ashcroft T, Simpson JM & Timbrell V Simple method of estimating severity of pulmonary fibrosis on a numerical scale. J. Clin. Pathol 41, 467–70 (1988). [PubMed: 3366935]

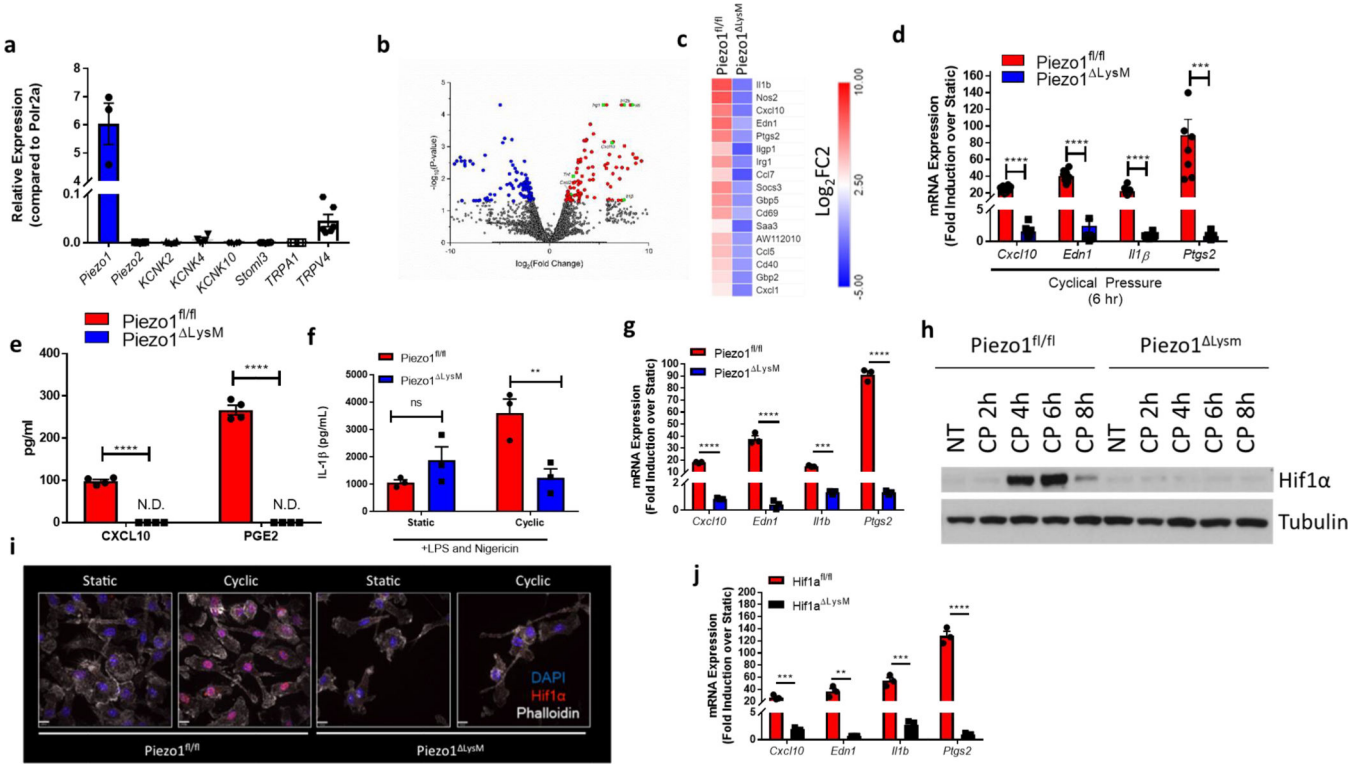

Figure 1: PIEZO1 Signaling in Macrophages Induces Transcriptional Reprogramming Via HIF1α

a, qPCR analysis of known mammalian mechanosensory ion channels from unstimulated BMDMs. Data is presented as 3 biological replicates from 2 independent experiments. **b,** Volcano plots showing differentially expressed genes comparing 6 hours of cyclic hydrostatic pressure and 6 hours static stimulated treated Piezo1$^{fl/fl}$ BMDMs **c,** HeatMap showing top genes upregulated by PIEZO1 signaling. Data is shown as Log_2 fold change of cyclical hydrostatic pressure over static pressure treated Piezo1$^{fl/fl}$ or Piezo1$^{\Delta LysM}$ BMDMs 6 hours post mechanostimulation **d,** qPCR analysis of top upregulated genes from BMDMs treated with 6 hours of cyclic hydrostatic pressure. Data is presented as 8 biological replicates from 3 independent experiments. **e,** ELISA of CXCL10 and PGE2 from supernatant of BMDMs cultured in cyclical hydrostatic pressure or static pressure for 6 hours. Data is presented as 4 biological replicates from 2 independent experiments. **f,** IL-1β levels from BMDMs treated with 5 hours of LPS (10 ng/mL) and 1 hour of nigericin (10 μM) in cyclic hydrostatic pressure or static pressure as measured by ELISA. Data is presented as 3 biological replicates. **g**, qPCR validation of top upregulated genes from purified mouse monocytes treated with 6 hours of cyclic hydrostatic pressure. Data is presented as 3 biological replicates. **h**, Representative immunoblot analysis of HIF1α and β-tubulin in BMDMs cultured in cyclical hydrostatic pressure. Blots are representative of 5 independent experiments. **i**, Confocal microscopy detection of HIF1α from BMDMs cultured in static or cyclical hydrostatic pressure for 6 hours. Data is representative of 2 independent experiments. **j**, qPCR analysis of Hif1a$^{fl/fl}$ and Hif1a$^{\Delta LysM}$ BMDMs treated with 6 hours of cyclical hydrostatic pressure. Data is presented as 3 biological replicates.

a,d-g,j, SEM of replicates is present for qPCR and ELISA data, and significance is determined by unpaired two-tailed t test (**p<0.01, ***p<0.001, ****p<0.0001).

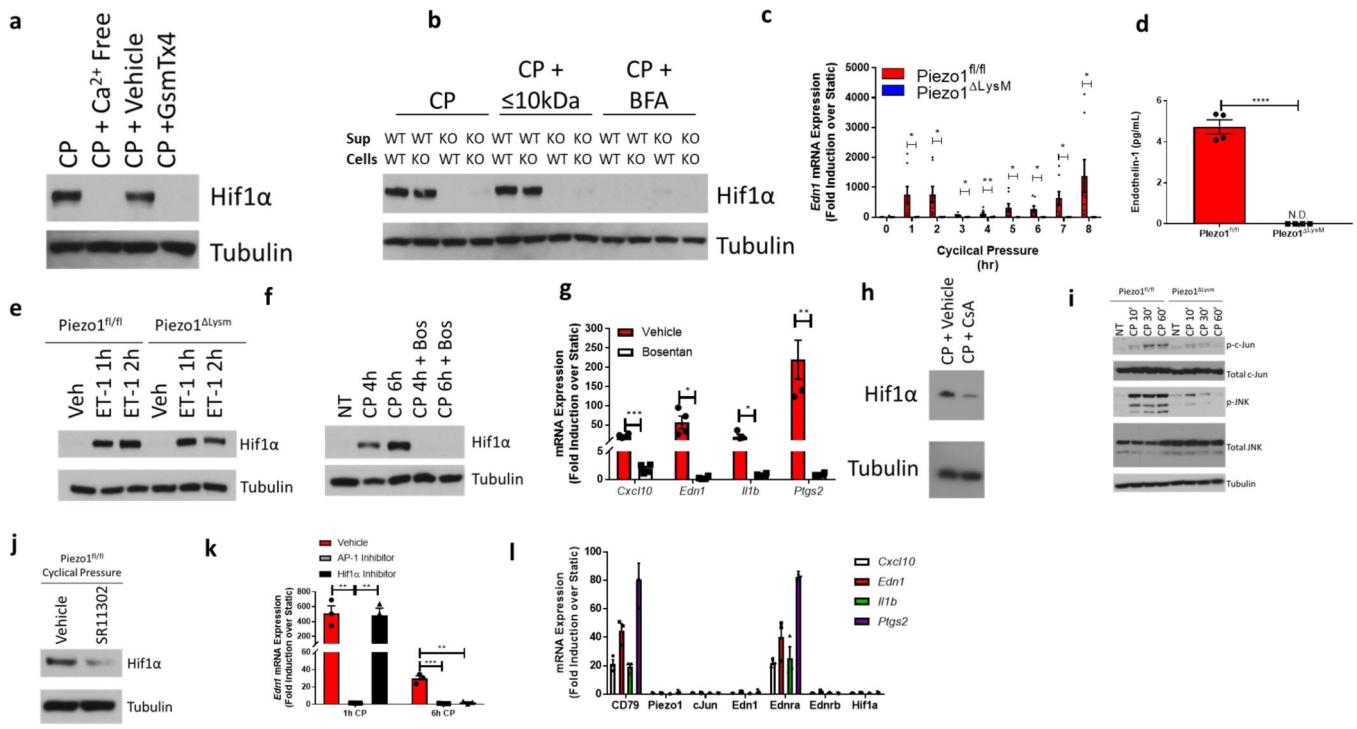

Figure 2: PIEZO1 Signaling Stabilizes HIF1α via EDN1

a, Representative immunoblot analysis of HIF1α and β-tubulin in BMDMs cultured in cyclical hydrostatic pressure for 6 hours with calcium-free media or with PIEZO1-inhibitor GsmT×4 (5 μM). Blots were representative of 2 independent experiments. **b**, Representative immunoblot analysis of HIF1α and β-tubulin in BMDMs. Supernatant from Piezo1$^{fl/fl}$ (WT) or Piezo1$^{\Delta LysM}$ (KO) cultured in cyclical hydrostatic pressure for 6 hours were transferred to WT or KO BMDMs cultured in static pressure for 2 additional hours. Molecules larger than 10 kDa were removed using a size-exclusion spin column. Secretion was inhibited using Brefeldin A (BFA) (3 μg/mL). Blots were representative of 2 independent experiments. **c**, qPCR analysis of *Edn1* from cyclical hydrostatic pressure treated BMDMs. Data is presented as 8 biological replicates from 3 independent experiments. **d,** EDN1 ELISA of supernatants from BMDMs treated in 6 hours of cyclical hydrostatic pressure. Data is presented as 4 biological replicates from 2 independent experiments. **e**, Representative immunoblot analysis of HIF1α and β-tubulin in BMDMs treated with recombinant endothelin-1 (ET-1, 10 nM). Blots were representative of 3 independent experiments. **f**, Representative immunoblot analysis of HIF1α and β-tubulin in cyclical hydrostatic pressure treated BMDMs in the presence of Bosentan (10 μM). Blots were representative of 3 independent experiments. **g**, qPCR analysis of Piezo1$^{fl/fl}$ BMDMs pretreated with Bosentan (10 μM) for 30 minutes prior to 6 hours of cyclical hydrostatic pressure. Data is presented as 4 biological replicates. **h**, Representative immunoblot analysis of HIF1α and β-tubulin in BMDMs pretreated with cyclosporine A (10 μM) for 30 minutes prior to 6 hours of cyclical hydrostatic pressure. Blots were representative of 2 independent experiments. **i**, Representative immunoblot analysis of phospho-c-JUN (p-c-JUN), phosphor-JNK (p-JNK), total c-JUN, total JNK, and β-tubulin in BMDMs cultured in cyclical hydrostatic pressure. Blots were representative of 3 independent experiments. **j**, Representative immunoblot

analysis of HIF1α and β-tubulin in BMDMs pretreated with AP-1 inhibitor SR 11302 (10 μM) for 30 minutes prior to 6 hours of cyclical hydrostatic pressure. Blots were representative of 2 independent experiments. **k**, qPCR analysis of *Edn1* from BMDMs pretreated with either AP-1 inhibitor SR 11302 (10 μM) or with echinomycin (5 nm) for 30 minutes prior to cyclical hydrostatic pressure treatment for 6 hours. Data is presented as 3 biological replicates. **l**, qPCR analysis of Cas9-KI BMDMs transduced with sgRNAs targeting the indicated gene of interest and treated with cyclical hydrostatic pressure for 6 hours. Data is presented as 3 biological replicates. **c,d,g,k,l,** SEM of replicates is present for qPCR and ELISA data, and significance is determined by unpaired two-tailed t test (*p<0.05, **p<0.01, ***p<0.001, ****p<0.0001).

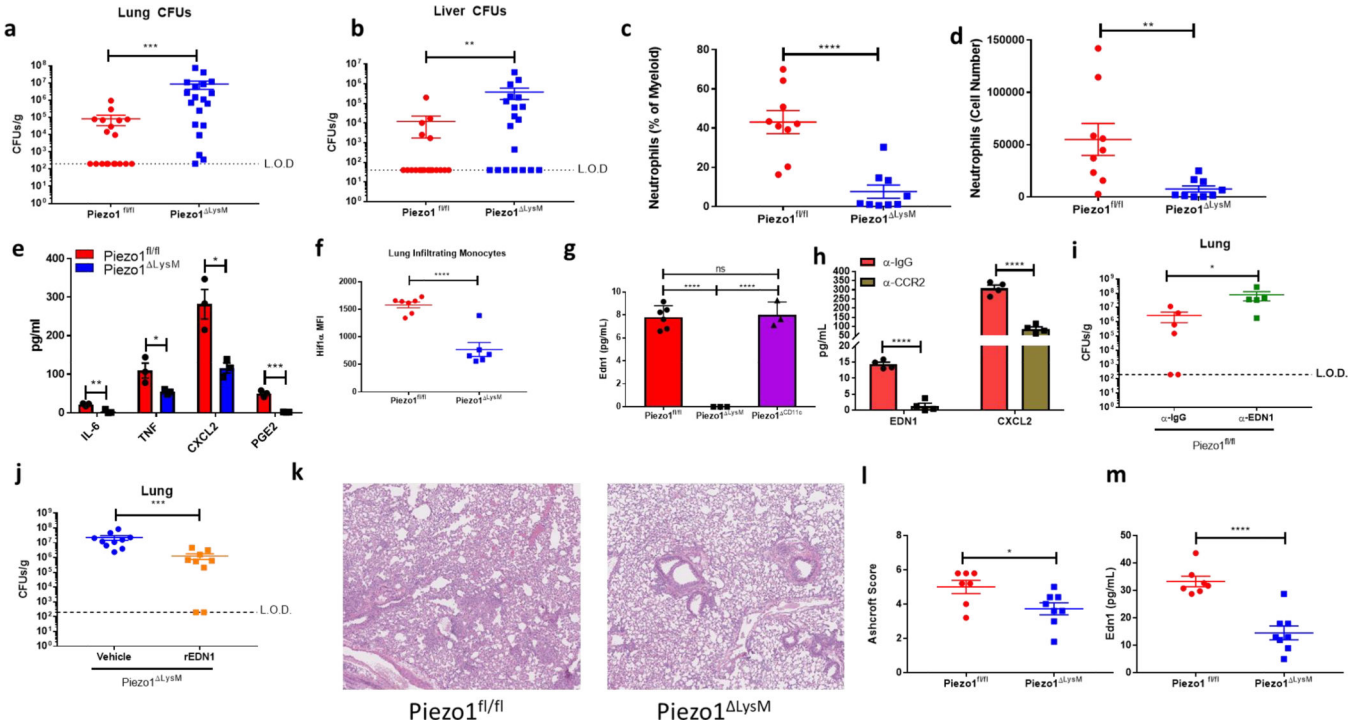

Figure 3: PIEZO1 Recognition of the Cyclical Hydrostatic Pressure Microenvironment in the Lung Drives Inflammation Via EDN1

a-b, Colony forming units (CFUs) from (**a**) lung and (**b**) liver of Piezo1$^{fl/fl}$ (n=19) or Piezo1$^{\Delta LysM}$ (n=19) mice infected intransally with *P. aeruginosa* for 24 hours. Data is from 4 independent experiments. **c-d,** Neutrophil quantification in terms of (**c**) percentage of myeloid and (**d**) total numbers from Piezo1$^{fl/fl}$ or Piezo1$^{\Delta LysM}$ lungs infected intranasally with *P. aeruginosa* for 6 hours. Data is from 2 independent experiments. **e,** ELISA quantification of indicated cytokines and PGE2 from BALF of Piezo1$^{fl/fl}$ and Piezo1$^{\Delta LysM}$ mice infected intranasally with *P. aeruginosa* for 2 hours. Data is presented as 3 biological replicates from 2 independent experiments. **f,** Mean fluorescent intensity (MFI) of HIF1α from total lung interstitial monocytes of Piezo1$^{fl/fl}$ (n=7) and Piezo1$^{\Delta LysM}$ (n=6) mice infected intranasally with *P. aeruginosa* for 6 hours. Data is from 2 independent experiments. **g,** Quantification of EDN1 by ELISA from BALF of Piezo1$^{fl/fl}$, Piezo1$^{\Delta LysM}$, or Piezo1$^{\Delta CD11c}$ vehicle-treated mice or infected intranasally with *P. aeruginosa* for 2 hours. Data is presented as 6 (Piezo1$^{fl/fl}$) or 3 (Piezo1$^{\Delta LysM}$ and Piezo1$^{\Delta CD11c}$) biological replicates. **h**, Quantification of EDN1 and CXCL2 by ELISA from BALF of mice depleted of monocytes with intraperitoneal α-CCR2 antibody (20 μg) or with isotype control 24 hours prior to infection. Data is presented as 4 biological replicates. **i**, CFUs from lung of Piezo1$^{fl/fl}$ mice infected intranasally with *P. aeruginosa* for 24 hours treated with α-EDN1 (ENDO20–2101.70, ThermoFisher) (25 μg) or isotype control intranasally 6 hours prior to infection. Data is from 2 independent experiments. **j**, CFUs from lung of Piezo1$^{\Delta LysM}$ mice infected intranasally with *P. aeruginosa* for 24 hours treated with vehicle (PBS) (n=10) or recombinant Endothelin-1 (rEDN1)(10ug) (n=9) intranasally at the time of infection. Data is from 2 independent experiments. **k**, Representative H&E staining of lung sections 14 days following intratracheal bleomycin treatment at 10× magnification. **l**, Average blinded

Ashcroft score of 5 fields of view from fixed lung tissue H&E stained 14 days following intratracheal bleomycin treatment at 10× magnification. Data is representative of 2 independent experiments. **m**, ELISA analysis of EDN1 levels from BALF 14 days following intratracheal bleomycin treatment. Data is representative of 2 independent experiments. **a,b,i,j,** SEM of replicates is present and significance is determined by Mann-Whitney U Test (**p<0.01,***p<0.001). **c-h,l,m,** SEM of replicates is present and significance is determined by unpaired two-tailed T test (*p<0.05, **p<0.01, ***p<0.001, ****p<0.0001).